AIAA JOURNAL
Vol. 50, No. 12, December 2012

Characterization of Aeroacoustic, Silicon Micromachined Microphones for Aircraft Fuselage Arrays

Matthew D. Williams,* Benjamin A. Griffin,† and Tiffany N. Reagan‡
University of Florida, Gainesville, Florida 32611-6250
James R. Underbrink§
The Boeing Company, Seattle, Washington 98108
and
Mark Sheplak¶
University of Florida, Gainesville, Florida 32611-6250

DOI: 10.2514/1.J051519

This paper describes the design and characterization of a micromachined microphone for aircraft fuselage arrays utilized by aeroacousticians to help identify aircraft noise sources and/or assess the effectiveness of noise-reduction technologies. The developed microphone utilizes piezoelectric transduction via an integrated aluminum nitride layer in a thin-film composite diaphragm fabricated using a combination of surface and bulk micromachining. The experimental characterization of several microphones is presented. Measured performance was in line with the Boeing Company specifications for the fuselage array application, including sensitivities of 32.1 μV/Pa to 43.7 μV/Pa, minimum detectable pressures as low as 40 dB (1 Hz bin at 1 kHz), confirmed bandwidths up to 20 kHz, >100 kHz resonant frequencies, and 3% distortion limits between 160 and 172 dB sound pressure level. With this performance, in addition to the small sizes, these microphones are shown to be a viable enabling technology for low-cost, high-resolution fuselage array measurements.

Nomenclature

c_0	=	isentropic speed of sound, m/s
d_a	=	effective acoustic piezoelectric coefficient, m^2/V
f_r	=	resonant frequency, Hz
$f_{\pm 2\,\mathrm{dB}}$	=	± 2 dB frequency bandwidth points, Hz
f^c	=	Cutoff frequency of plane wave tube, Hz
H_m	=	microphone frequency response, V/Pa
k	=	Boltzmann's constant, 1.38×10^{-23} J/K
MDP	=	minimum detectable pressure, dB
PMAX	=	$p_{\max}$, dB
$p_{\max}$	=	pressure level at distortion limit, Pa
$p_{\min}$	=	minimum detectable pressure, Pa
R_{ep}	=	resistance of the piezoelectric layer, Ω
S_m	=	microphone sensitivity taken at 1 kHz, V/Pa
S_r	=	reference microphone sensitivity taken at 1 kHz, V/Pa
S_a^i	=	current noise power spectral density of the buffer amplifier, A^2/Hz
S_a^v	=	voltage noise power spectral density of the buffer amplifier, V^2/Hz
S_o^v	=	total output voltage noise power spectral density of the microphone, V^2/Hz

Received 11 August 2011; revision received 8 January 2012; accepted for publication 1 March 2012.

*Graduate Research Assistant, Department of Mechanical and Aerospace Engineering, Interdisciplinary Microsystems Group; currently Sandia National Laboratories, Senior Member of Technical Staff.

†Postdoctoral Associate, Department of Mechanical and Aerospace Engineering, Interdisciplinary Microsystems Group; currently Sandia National Laboratories, Senior Member of Technical Staff.

‡Graduate Research Assistant, Department of Mechanical and Aerospace Engineering, Interdisciplinary Microsystems Group.

§Boeing Technical Fellow, Aero/Noise/Propulsion Laboratory. Member AIAA.

¶Professor, Department of Mechanical and Aerospace Engineering, 231 MAE-A, P.O. Box 116250. Associate Fellow AIAA.

I. Introduction

AIRCRAFT manufacturers increasingly face regulatory and market-driven pressures to reduce aircraft noise. In the United States, the Federal Aviation Administration dictates noise standards that aircraft must meet in order to receive airworthiness certification [1], while noise standards also continue to grow more stringent abroad [2]. Passenger expectations for a quiet flight experience [3] coupled with concern about long-term noise exposure of flight crews [4] also drive aircraft manufacturers to reduce cabin noise in-flight.

During the aircraft component design and redesign process, aeroacousticians use advanced experimental technologies to help guide noise-reduction efforts [5]. Chief among these technologies are microphone arrays, which are distributed collections of microphones that spatially sample pressure fluctuations. Arrays with different purposes are deployed: dynamic pressure arrays capture hydrodynamic pressure fluctuations associated with a turbulent boundary layer and incident acoustic pressure fluctuations, while aeroacoustic phased arrays are used to resolve noise sources via a family of postprocessing techniques known as beamforming algorithms.

Arrays were utilized heavily in the 2005–2006 Quiet Technology Demonstrator 2 program, which brought together a consortium of aerospace industry leaders (including the Boeing Company, General Electric Aircraft Engines, Goodrich Corporation, the National Aeronautics and Space Administration, and All Nippon Airways) for a series of tests to evaluate noise-reduction technologies [6,7]. A goal of the tests was to determine the effectiveness of various engine inlet and exhaust configurations at reducing noise transmitted to the cabin or radiated to the community below. Both full-scale flight tests using dynamic pressure arrays and static engine tests using phased arrays were conducted. A dynamic pressure array featuring Kulite LQ pressure transducers [8] surface mounted on the exterior of a Boeing 777 is pictured in Fig. 1. The array enabled the spectral mapping of pressure fluctuations associated with the boundary layer and "shockcell noise" (a large contributor to aft interior cabin noise) along the fuselage, comparison of levels before and after engine treatments, and the identification of axial fuselage locations subjected to the highest shockcell noise levels [9]. A similar array was deployed forward of the engines for the characterization of "buzzsaw noise" [6]. The deployment of phased arrays in static engine tests, with their lower cost and complexity compared to flight tests, enabled a more comprehensive assessment of noise-reduction

technologies via the inclusion of more engine configurations and instrumentation. Instrumentation for these tests include Brüel and Kjær 4938 1/4 in. pressure field microphone in the phased arrays and Kulite LQ pressure transducers flush mounted on the engine.

Full-scale flight tests and static engine tests are regular events at the Boeing Company. Limitations exist in the deployment of high-channel-count arrays, including the cost per channel, data collection and storage capabilities, and compatibility with existing test facilities [10]. In addition, microphones used in aeroacoustic array measurements must often meet demanding requirements, including the sensing of high sound pressure levels (>160 dB) with low distortion (<3%) and high sensitivity stability (100ths of a decibel). Measurement-grade sensors that meet these criteria are expensive, often costing upwards of $2000. With unavoidable equipment loss due to measurements performed outdoors and in the harsh high-altitude environment of flight tests, the large initial investment gives way to significant recurring costs as well.

Microphones based on the technology of microelectromechanical systems (MEMS) show promise for meeting the stringent performance needs of aeroacoustic applications at reduced cost, made possible using batch fabrication technology [11–18]. Higher density arrays with better performance become possible when channel cost is reduced. Perhaps most importantly, the small size of MEMS microphones position them as an enabling technology for more advanced measurements, particularly in full-scale flight tests where sensors must be extremely thin and robust. Beyond cost contraints, the Kulite microphones composing the array in Fig. 1 are sparsely distributed because sensor locations must be carefully chosen to avoid flow disturbances caused by upstream sensors affecting those downstream. With these sensor density restrictions, deployed arrays have been insufficient for beamforming [19]. Thinner sensors with smaller packaging may be more densely packed, enabling both higher-resolution maps of the fluctuating pressure field on the fuselage and, eventually, the beamforming of in-flight data to identify dominant noise sources for actual—not simulated—flight conditions.

This paper discusses the design and characterization of MEMS microphones appropriate for use in aeroacoustic arrays. The primary application for this work is the fuselage array. Static engine test arrays, with less stringent specifications in many respects, are viewed as a secondary application. First, Sec. II provides an overview of the microphone technology used in this study and briefly describes the microphone design. Section III describes the fabrication of the microphones and Sec. IV addresses their packaging for laboratory characterization. Section V describes the experimental characterization of several microphones, and finally, Sec. VI offers conclusions and directions for future work.

Fig. 1 Boeing 777 fuselage instrumented with an array of microphones. (Courtesy Boeing.)

Table 1 Fuselage array application requirements

Metric	MEMS requirement	Kulite LQ
Sensing element size	$\phi \leq 1.9$ mm	864 μm × 864 μm
Sensitivity	500 μV/Pa[a]	1.1 μV/Pa
Min. detectable pressure	$\leq$ 48.5 dB[b]	48.5 dB[b]
	$\leq$ 93 dBOASPL[c]	93 dB OASPL[c]
Max. pressure[d]	$\geq$ 172 dB	172 dB
Bandwidth	20 HZ–20 kHz[e]	<20 Hz–20 kHz+

[a]With on-board gain.
[b]1 Hz bin centered at 1 kHz.
[c]20 Hz–20 kHz.
[d]3% distortion.
[e]±2 dB.

II. Overview

This section provides an overview of the microphone technology used in this study and the desired performance. The project sponsor, the Boeing Company, established design targets for the fuselage array application, found in Table 1. These requirements were derived from the desire to meet or exceed existing measurement capabilities of the Kulite LQ pressure transducers, whose performance characteristics are also collected in Table 1.

Among the transduction mechanisms available for microfabricated microphones are capacitive [15–17], piezoresistive [11,12,15,16], optical [18], and piezoelectric [14]. Beyond the performance requirements in Table 1, low power consumption is an important goal because it enables the use of compact data acquisition systems with common integrated 4 mA constant-current sources. Piezoelectric transduction does not require a bias voltage and also offers the appropriate combination of ruggedness, simplicity, and performance. It is therefore used in the microphone design described here.

The microphone structure is composed of a circular diaphragm with a metal/piezoelectric/metal film stack situated on the high stress/strain region around its outer boundary. A depiction (not to scale) of the microphone structure is shown in Fig. 2 with a quarter cutout. The diaphragm deflects under an incident acoustic pressure wave, and the resulting stress/strain in the piezoelectric material yields a proportional output voltage. The diaphragm is composed of passivation, electrode, piezoelectric, and structural layers and is front side vented. Aluminum nitride was used in lieu of more common thin-film piezoelectrics like lead zirconate titantate or zinc oxide due to its attractive properties, including a high material figure of merit for sensitivity (g_{31}), low dielectric loss, and high intrinsic signal-to-noise ratio [20].

The design and optimization of the microphones were accomplished via the use of the lumped element modeling approach [14,21] together with a piezocomposite diaphragm model, with both integrated into a single-objective optimization algorithm. Whereas design details are given elsewhere [22], the primary drivers are briefly summarized here. The main conflicting requirements were to

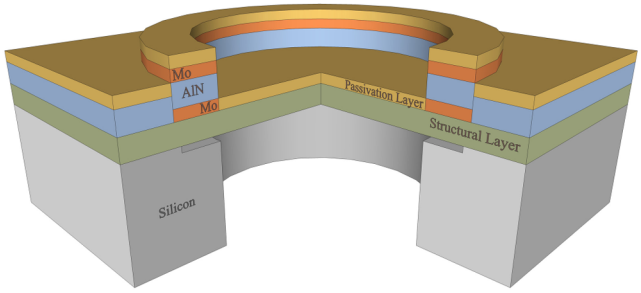

Fig. 2 Microphone structure with quarter cutout (not to scale), featuring a circular diaphragm with an annular electrode/piezoelectric/electrode ring.

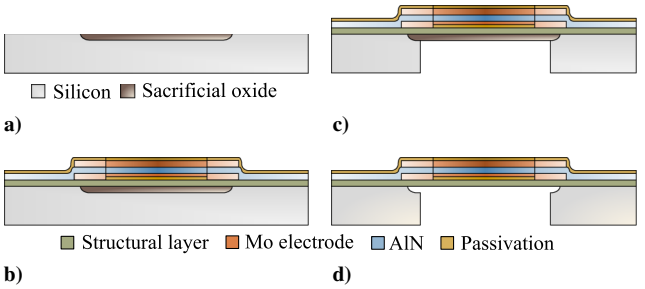

Fig. 3 Microphone fabrication process.

achieve a very high 3% distortion limit, $p_{\max} \geq 172$ dB, and the lowest possible minimum detectable pressure, $p_{\min}$. The former is accomplished via the selection of a sufficiently stiff diaphragm. Meanwhile, the minimum detectable pressure (MDP) is more nuanced. Under the conditions that the dominant noise contributors are the buffer amplifier and dielectric loss, the expression for $p_{\min}$ may be written as [22]

$$p_{\min} \approx \sqrt{\int_{f_1}^{f_2} \left[\frac{S_a^i + \frac{4\ \mathrm{kT}}{R_{ep}}}{(\omega d_a)^2} + \frac{S_a^v C_{et}^2}{d_a^2} \right] \mathrm{d}f} \tag{1}$$

where the integration $f_1 \rightarrow f_2$ is over a bandwidth of interest, S_a^i is the current noise power spectral density (in amperes squared per hertz) of the amplifier, S_a^v is the voltage noise power spectral density (volts squared per hertz) of the amplifier, k is Boltzmann's constant, T is temperature, R_{ep} is the electrical resistance associated with the piezoelectric layer in the annular film stack, C_{et} is the total capacitance of the microphone, and d_a (meters cubed per volt) is the effective acoustic piezoelectric coefficient. From Eq. (1), it is desirable to have high piezoelectric coupling (d_a), high resistance in the piezoelectric layer (R_{ep}), and low noise from the amplifier (S_a^i and S_a^v). The properties d_a and R_{ep} are tied to each other via the choice of material and design of the annular film stack (i.e., thickness and area). In addition, d_a also trends similarly to the compliance of the diaphragm.

Taking all of these tradeoffs into account, seven microphone designs labeled A through G were produced with $p_{\min}$ and $p_{\max}$ predictions in the vicinity of the targets given in Table 1. Film thicknesses were the same for all designs, and the width of the annular film stack varied little; meanwhile, the outer diameters varied significantly from 514 μm to 910 μm.

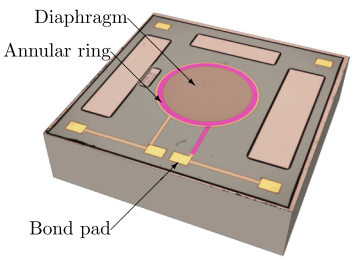

Fig. 4 Microphone die (2 mm on a side) of design F (diameter of 828 μm)

III. Fabrication

Fabrication was performed at Avago Technologies using a variant of their film bulk acoustic resonator (FBAR) process [23–25], more commonly used to produce duplexers and filters for cellular phones. Although exact FBAR process details are proprietary, a general outline of fabrication steps for a microphone structure was published by Avago Technologies [24,25] and is summarized in Fig. 3. The process involved both surface and bulk micromachining, starting with a 675-μm-thick, 150 mm (6 in.) silicon wafer. First, a shallow cavity was etched and filled with sacrificial material, which served to define the diaphragm diameter and set an etch stop for subsequent backside processing. The wafer surface was thinned to 500 μm and planarized via chemical-mechanical polishing (CMP) as shown in Fig. 3a. The structural, metal (molybdenum), piezoelectric, and passivation layers, in addition to the bond pads, were then deposited and patterned in a set of proprietary process steps (Fig. 3b). The materials used in the passivation and structural layers were proprietary features of the process and are thus not disclosed. Projection step-and-repeat photolithography was used to repeat the same 10 × 10 pattern of microphones over the entire wafer. A deep reactive ion etch (DRIE) from the backside of the wafer formed the back cavity (Fig. 3c) and the sacrificial material was removed to release the diaphragm (Fig. 3d).

All seven microphone designs discussed in Sec. II were fabricated. This paper presents the experimental results for the more acoustically sensitive designs D, E, and F, with outer diameters of 690 μm, 756 μm, and 828 μm, respectively. A microphone die of design F is shown in Fig. 4; die dimensions are 2 mm on a side.

IV. Packaging

The packaging of the MEMS piezoelectric microphone for use in fuselage arrays requires a small, thin, and inexpensive solution. A package that meets all of the requirements for deployment in the field demands significant development and is beyond the scope of this study. However, laboratory test packaging that enables seamless transition of the MEMS microphone into multiple test setups among the research laboratory and project sponsor is also an important development. This section describes the creation of a laboratory test package that is compatible with common test fixtures for 1/4 in. microphones at both the Interdisciplinary Microsystems Group and the Boeing Company. An in-depth look at the Boeing Company flush-mount adapter designs is found elsewhere [26].

The entire package was composed of structural and connectivity components as shown in the exploded view of Fig. 5. The microphone die was epoxied into a circular printed circuit board (to be called the "endcap") and gold wire bonds were made from bond pads on the die to vias on the endcap. The endcap was connected to the end of a brass tube via alignment pins. A circuit board with a

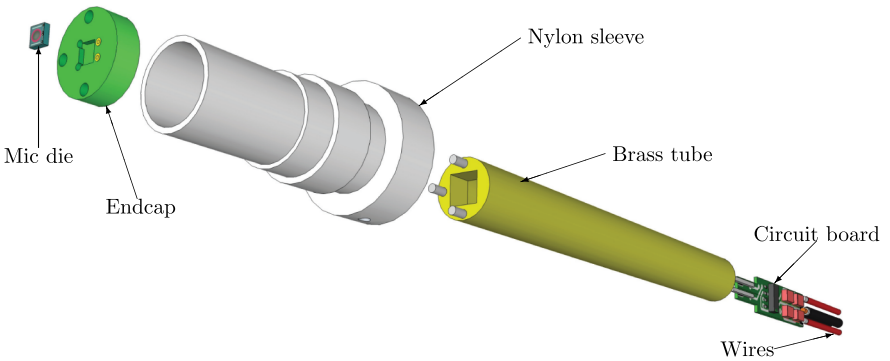

Fig. 5 Exploded view of the laboratory test package.

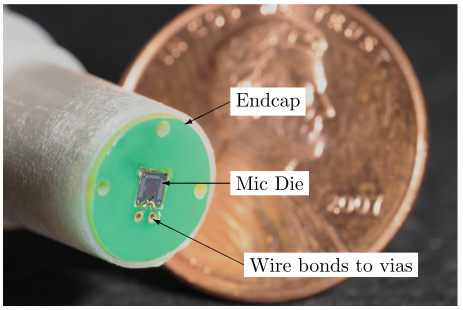

Fig. 6 Closeup photograph of a packaged MEMS piezoelectric microphone.

buffer amplifier was housed inside the brass tube, and it was interfaced to the endcap via solder connections. Wire connections to the circuit board for transmitting the microphone output and powering the buffer amplifier emerged from the back side of the brass tube. A nylon sleeve was fixed on the assembled brass tube and endcap via set screws in the thickest part of its base and served to electrically isolate the brass tube from test fixtures, while also ensuring mounting flushness. Finally, heat shrink tubing (not shown) was used to stress relieve the wires protruding from the brass tube. Brass tubes and nylon sleeves were provided by the Boeing Company. A packaged microphone is shown in Fig. 6.

V. Experimentation

This section describes the experimental characterization of five MEMS piezoelectric microphones of three different designs. The measurements of the resonant frequencies, frequency response, linearity, and noise floor are presented.

A. Resonant Frequency

The resonant frequency, f_r, of a microphone provides a qualitative measure of bandwidth in the absence of high-frequency acoustic characterization. Microphone die excited using a broadband electrical signal were interrogated using a single-point measurement beneath a laser vibrometer (LV). Each die was interrogated only at a single point in the center of the diaphragm to maximize the LV signal. A periodic chirp signal over a frequency range from 0 to 200 kHz with resolution of 31.25 Hz was used, and f_r was selected from the maximum of the displacement per voltage frequency response function. The results of the resonant frequency measurements are found in Table 2, with f_r decreasing with increasing diaphragm size (D $\rightarrow$ F) as expected. All devices exhibited $f_r > 100$ kHz.

B. Frequency Response

The frequency response of the piezoelectric microphones, $H_m(f)$ (volts per pascal), was determined over the audio range via comparison with a measurement-grade reference microphone. Different frequency bands were measured at the University of Florida and the Boeing Company facilities.

At the University of Florida, the acoustic characterization was performed in an approximately 1-m-long, 2.2-cm-thick, aluminum plane wave tube (PWT) with a 1 in. $\times$ 1 in. duct. A PWT is a rigid waveguide designed such that only planar waves propagate below its cutoff frequency, f^c, which is dependent on cross-sectional geometry and the isentropic speed of sound c_0 of the associated gas. Two

Table 2 Resonant frequency measurements

MEMS mic	f_r, kHz
E4-D	132.6
I2-D	133.5
I8-E	114.4
H3-F	103.9
J3-F	103.9

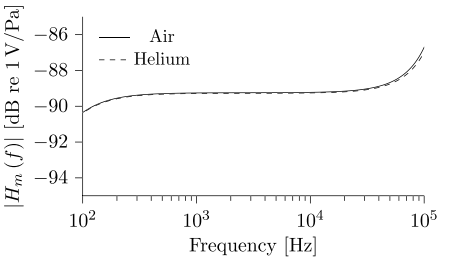

Fig. 7 Predicted frequency response magnitude in air and helium for design D.

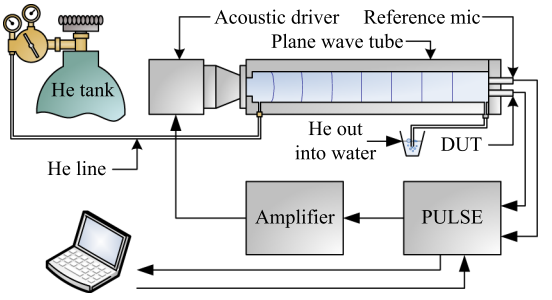

Fig. 8 PWT setup for acoustic characterization.

microphones mounted at the same lengthwise location are simultaneously exposed to the same pressure for drive frequencies less than f^c. Complementary frequency response measurements were performed using both air and helium in the PWT, for which f^c is 6.7 kHz and 19.8 kHz, respectively. The measurement in air was intended to yield accurate sensitivity information under normal operating conditions. The expanded frequency range of the helium measurement enabled the assessment of the flatness of the frequency response over nearly the full audio range. The use of helium, instead of air, has a slight effect on the performances of both the MEMS microphones and the reference microphone. For example, a helium-filled cavity is less compliant than an air-filled cavity. A lumped element model for the microphone frequency response [22] yields a predicted flat band sensitivity of

$$S = \frac{\phi_a}{\phi_a^2 + \frac{C_{et}}{C_{ad}}\left(1 + \frac{C_{ad}}{C_{ac}}\right)} \tag{2}$$

where C_{ad} is the acoustic compliance of the diaphragm and ϕ_a is the transduction factor. The acoustic compliance of the cavity, C_{ac}, is inversely proportional to the bulk modulus of the associated gas. In general, $C_{ad}/C_{ac} \ll 1$ and, thus, the cavity composition has minimal impact on the frequency response, as shown in Fig. 7 for design D in air and helium. Depending on the microphone design, the reduction in sensitivity in helium compared to air was predicted to be 0.04 dB to 0.4 dB.

The experimental setup is shown in Fig. 8, with both the reference microphone and single MEMS microphone (the device under test [DUT]) mounted at the end of the PWT. The reference microphone used was a Brüel and Kjær 4138 1/8 in. pressure field microphone. A Brüel and Kjær Type 3560D Multichannel Portable PULSE system was used to generate the test signal and acquire data. The pseudorandom test signal was ampified via a Techron 7540 power amplifier prior to reaching a BMS 4590 compression driver. The pseudorandom noise excitation signal with the frequency content above 300 Hz was used due to the poor response of the compression driver below that frequency. Measurement settings are collected in Table 3. For the helium measurement, the PWT was flooded with helium via a pressurized canister regulated at 10 psi. The helium exited the PWT into a cup of water.

In air, the frequency response of a MEMS microphone, $H_m(f)$, was determined simply as the frequency response function relating

its output (volt) and the output of the calibrated reference microphone (pascal). The reference microphone frequency response magnitude was regarded as flat in this calculation and only relative phase was determined. In helium, concerns about the stratification of the gas medium and resulting wavefront distortion led to the use of the substitution method to improve measurement quality. This method required two frequency response measurements with the microphones in original and swapped positions. Let H^o_{rm} and H^s_{rm} represent the measured frequency response functions in the original and swapped positions, respectively, relating the output of microphone m (a MEMS microphone) to that of microphone r (the reference) in units of V/V. Under the assumption that there is no change in the pressure field between measurements, the DUT frequency response function V/Pa is found from [13,27]

$$H_m = S_r \sqrt{H^o_{rm} H^s_{rm}} \tag{3}$$

where S_r is the sensitivity of the reference microphone. Therefore, the frequency response function of a MEMS microphone, $H_m(f)$, is deduced from the geometric mean of measurements for H^o_{rm} and H^s_{rm} even when the two microphones are not exposed to precisely the same pressure.

The frequency response function measurements made in helium are collected in Fig. 9, shown in terms of magnitude and relative phase. The frequency response magnitude is flat to well within the stated goal of ±2 dB from 300 Hz to 20 kHz. Deviations in the magnitude and phase close to 20 kHz are the result of the onset of higher-order acoustic mode propagation. Note that the phase is relative to the reference microphone. The microphones were phase matched to <2 deg out to 19 kHz.

The sensitivities of the MEMS microphones are collected in Table 4 in both dB and μV/Pa for measurements performed in air. The sensitivities in helium were all lower than in air by less than 0.2 dB (2.3%). The phase rolloff in helium was less than in air by approximately 5 deg at 6 kHz.

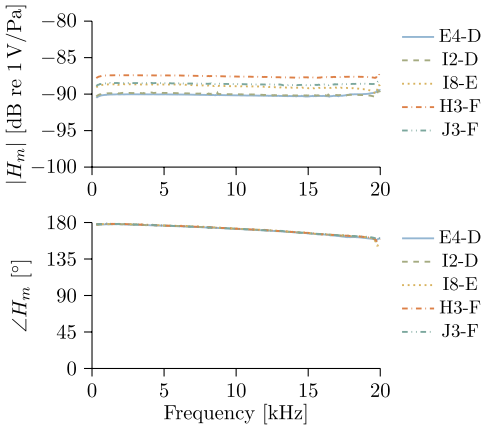

Fig. 9 Microphone frequency responses in helium.

Table 4 Microphone frequency response characteristics[a] at 1 kHz in air

	Magnitude		
MEMS mic	dB re 1 V/Pa	μV/Pa	Relative Phase (deg)
E4-D	−89.86 ± 0.06	32.1 ± 0.2	177.3 ± 0.1
I2-D	−89.77 ± 0.06	32.5 ± 0.2	177.9 ± 0.1
I8-E	−88.71 ± 0.06	36.7 ± 0.2	178.1 ± 0.1
H3-F	−87.19 ± 0.06	43.7 ± 0.3	178.3 ± 0.2
J3-F	−88.25 ± 0.06	38.7 ± 0.3	178.0 ± 0.2

[a]Uncertainties are for 95% confidence interval.

Because of the low-frequency limitations of the BMS 4590 compression driver used in the PWT setup, additional measurements to characterize the low-frequency rolloff of the piezoelectric microphone were performed at the Boeing Company. Two piezoelectric microphones, I2-D and J3-F, were transferred to the Boeing Company for this measurement and others. The measurement setup is pictured in Fig. 10 and consisted of the MEMS and Brüel and Kjær 4136 reference microphone mounted in a small acoustic cavity (Fig. 10b shows two mounted Brüel and Kjær 4136 microphones) that was driven by a speaker and terminated into an "infinite" (100 ft) copper tube. The infinite tube termination provides an essentially anechoic termination and as such supports only forward-propagating acoustic waves. The primary assumption of this measurement setup is that the two microphones are exposed to the same pressure over the frequency range of interest, which was confirmed via a measurement made using two Brüel and Kjær 4136 microphones.

In performing the experiment an HP 35670 spectrum analyzer provided a broadband white noise signal and acquired the MEMS and reference microphone signals over a bandwidth of 0 kHz to 1.6 kHz with a frequency resolution of 1 Hz. Using the spectrum analyzer, the frequency response function relating the DUT output to the calibrated reference microphone output (volts per pascal) was calculated. The frequency response function was then postprocessed to correct for the low-frequency rolloff in the reference microphone. The low-frequency calibration of the reference microphone was obtained at 1/3 octave bands down to 10 Hz using a Brüel and Kjær UA0033 electrostatic actuator. At frequencies (<800 Hz), the accuracy of this method is approximately 0.5 dB [28]. The typical −3 dB lower-limiting frequency for a Brüel and Kjær 4136 is 0.3 Hz to 3 Hz.

The normalized frequency response measurements are captured in Fig. 11. Both −2 dB and −3 dB frequencies are collected in Table 5 with associated uncertainties given ±0.5 dB accuracy in the reference microphone electrostatic calibration. The nominal −2 dB frequencies were above the target of 20 Hz for both microphones.

C. Linearity

The characterization of microphone linearity refers to the quantification of how the voltage output of the MEMS microphones change with sound pressure level. Measurements were performed at both the University of Florida and at the Boeing Company. From the collected

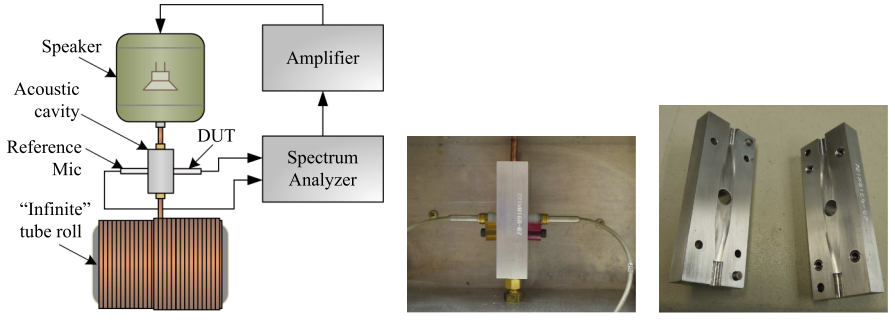

Fig. 10 Infinite tube measurement setup: a) measurement schematic, b) two Brüel and Kjær 4136 microphones mounted in the acoustic cavity, and c) inside the acoustic cavity.

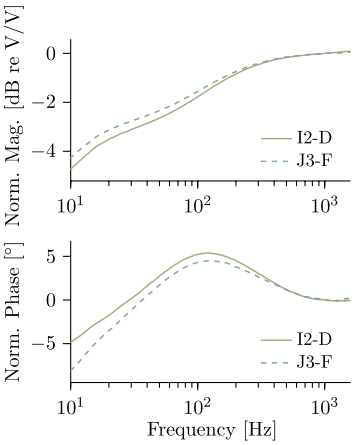

Fig. 11 Piezoelectric microphone frequency response functions at low frequencies normalized to values at 1 kHz.

data, total harmonic distortion was calculated in terms of power spectral density as [29]

$$\mathrm{THD} = \sqrt{\frac{\sum_{n=2}^{\infty} G_{mm}(f_n)}{G_{mm}(f_1)}} \times 100\% \tag{4}$$

where f_1 is the fundamental frequency, excitation frequency, or first harmonic, and f_n is the nth harmonic. Assuming uniform microphone sensitivity at each f_n, the power spectral density of the MEMS microphone output, G_{mm}, can be regarded in units of $\mathrm{Pa}^2/\mathrm{Hz}$ or V^2/Hz.

At the University of Florida, the same setup used to find the frequency response (in air), pictured in Fig. 8, was used to obtain data for the total harmonic distortion calculation. A single tone signal at 1 kHz drove the BMS 4590 compression driver, which could reach a sound pressure level (SPL) of approximately 160 dB without exceeding its power rating. A PCB Piezotronics Model 377A51 precision condenser microphone, with a maximum SPL of 192 dB (3% distortion) served as the reference. The MEMS and reference microphone output signals were collected using the same settings found in Table 3 at multiple pressure levels. Starting from the lowest SPL with a detectable second harmonic, the SPL was increased in steps of 3–4 dB SPL up to 160 dB. The 6.4 kHz bandwidth enabled the first six harmonics to be captured. For this PWT measurement it is important to recognize that since harmonics above the sixth propagate as higher order modes, they do not contribute equally to the DUT and reference microphone responses. Therefore, power distributed to frequencies f_n for $n > 6$ must be negligible in order for the calculation to be valid.

Figure 12 is a plot of the MEMS microphone voltage output versus the reference microphone pressure (both taken at the fundamental frequency of 1 kHz). The response to each of the microphones was highly linear, with $R^2 > 0.99$.

Figure 13 shows the total harmonic distortion (THD) calculation for one representative microphone, J3-F. The large level of distortion (30–40%) for the reference microphone, which by specification does not exceed 3% until 192 dB, indicates the measurement environment is harmonic rich. Nonlinearities in the amplifier, speaker, and acoustic propagation path are all possible contributors. As a result, the calculated THD of Fig. 13 is not valid in an absolute sense, though the comparison of the calculations for the MEMS and reference microphones provides valuable qualitative information. The THD of

Table 5 Lower-limiting frequencies

Microphone	−2 dB	−3 dB
I2-D	85 $\mathrm{Hz}^{+35\ \mathrm{Hz}}_{-28\ \mathrm{Hz}}$	34 $\mathrm{Hz}^{+23\ \mathrm{Hz}}_{-14\ \mathrm{Hz}}$
J3-F	69 $\mathrm{Hz}^{+35\ \mathrm{Hz}}_{-28\ \mathrm{Hz}}$	22 $\mathrm{Hz}^{+19\ \mathrm{Hz}}_{-7\ \mathrm{Hz}}$

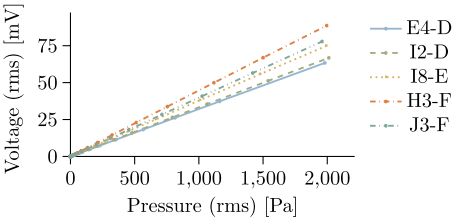

Fig. 12 Linearity measurements.

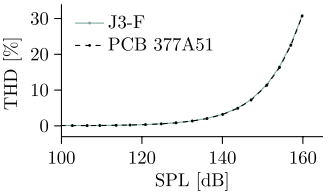

Fig. 13 THD measurements for microphone J3-F.

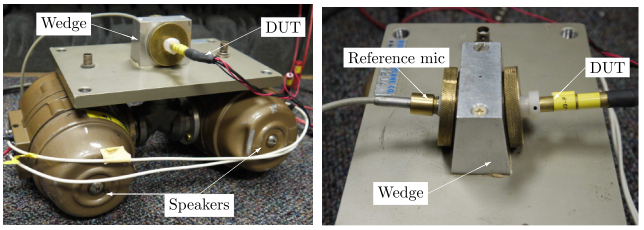

a) **b)**

Fig. 14 Linearity measurement setup at the Boeing Company: a) view of the entire wedge fixture, with speakers; and b) reference microphone and DUT mounted in the wedge.

MEMS microphone J3-F and the reference align closely, with a maximum observed difference of 0.3% THD. The same close agreement was observed for all other MEMS microphones as well, providing reasonable certainty that the 3% distortion limit significantly exceeds 160 dB.

A measurement setup at the Boeing Company was designed specifically to minimize harmonic contamination at high sound pressure levels. Photographs of the setup are found in Fig. 14. The measurement apparatus, known as "the wedge," houses a low-volume acoustic cavity driven by four manifolded speakers. A reference microphone (in this case the Brüel and Kjær 4938 $\frac{1}{4}$ in. pressure field microphone with 172 dB distortion limit) and the MEMS microphone were mounted facing each other, as shown in Fig. 14b), at close proximity (0.231 in.). A single tone excitation signal at 2.5 kHz was used, and the maximum achievable SPL in the wedge was approximately 172 dB. An HP35670A spectrum analyzer was used to collect the data and perform the THD calculation with 10 harmonics included. The frequency resolution was 64 Hz.

The results of the Boeing Company linearity measurements are collected in Table 6. The calculated total harmonic distortion in both the MEMS and reference microphone are given for each test,

Table 6 THD measurements performed at the Boeing Company

Measurement	Microphone	SPL (dB)	THD (%)
1	I2-D	166.0	3.0
	Brüel and Kjær 4938	167.6	2.4
2	J3-F	171.6	2.9
	Brüel and Kjær 4938	171.3	11.5

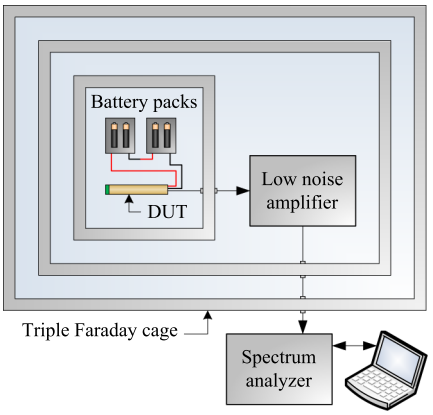

Fig. 15 Triple Faraday cage setup for noise floor characterization.

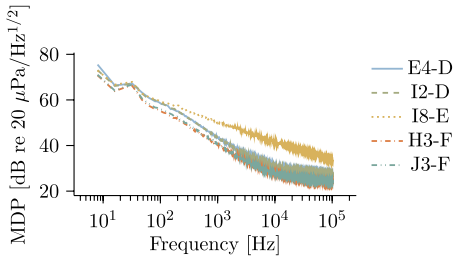

Fig. 16 MDP spectra.

and SPLs are reported as the pressure measured at 2.5 kHz (the fundamental frequency) using each microphone. Using the Brüel and Kjær 4938 and the MEMS microphone to measure SPL while they distort yields reported SPL estimates that are biased low. That is, reported distortion occurs at a SPL greater than that given here. Therefore, the device J3-F almost certainly meets the 172 dB specification for 3% distortion limit.

Table 7 MDP metrics

MEMS mic	dB SPL[a]	dB OASPL[b]	dB (A) OASPL[c]
E4-D	43.5	85.3	78.3
I2-D	43.9	85.3	78.2
I8-E	50.6	89.2	86.3
H3-F	40.2	82.7	75.0
J3-F	40.4	83.2	75.4

[a]Narrow bin ($f = 1$ kHz, $\Delta f = 1$ Hz); $|U_{95\%}| < 0.10$ dB.
[b]$|U_{95\%}| < 0.01$ dB.
[c]$|U_{95\%}| < 0.007$ dB (A).

D. Noise Floor

This section details the measurement strategy for the microphone's intrinsic noise floor. The intrinsic noise floor is of primary importance because it indicates the best achievable noise characteristics of the MEMS microphones when effectively shielded from extrinsic noise sources (e.g., electromagnetic interference). Referring the intrinsic electrical output noise to the microphone input yields the MDP of the microphone.

The measurement setup [30] using a triple Faraday cage is pictured in Fig. 15. The triple Faraday cage serves to attenuate electromagnetic interference from the laboratory environment. The MEMS microphone was battery powered in the innermost Faraday cage, with its output signal amplified 1000 times by a Stanford Research Systems (SRS) Model SR560 Low-Noise Preamplifier, also battery powered. A SRS Model SR785 2 Channel Dynamic Signal Analyzer was used to measure the output power spectral density (volts squared per hertz) over a bandwidth from 0 Hz to the maximum frequency of 102.4 kHz using multiple spans due to data acquisition limits. Between 1 k and 10 k, blocks were collected depending on the span, and the data was averaged using a Hanning window and 75% overlap. Bandpass filtering with the SR560 was done from 0.03 Hz–300 kHz. The SR560 noise floor was measured independently via the shorting of the input and was subtracted, in terms of power spectral density (PSD), from the MEMS microphone output before the noise was input referred.

Figure 16 shows the MDP spectra of the microphones, calculated from the measured output noise PSD, S_o^v, as

$$\mathrm{MDP} = 20\log_{10}\left(\frac{\sqrt{S_o^v/|S_m|^2}}{20\ \mathrm{Pa/Hz^{1/2}}}\right) \tag{5}$$

where $|S_m| = |H_m(1\ \mathrm{kHz})|$ from Sec. V.B. Because $|S_m|$ is a flat band sensitivity value, this calculation is not valid below f_{-2} and above f_{+2}.

Figure 16 shows the MDP spectra for the five measured devices. The noise floor in the audio band is seen to be below 70 dB for all microphones and below the target 1 kHz narrow bin MDP of 48.5 dB, save for the outlier, I8-E. By 20 kHz, MDP declines to approximately 25 dB SPL.

From the data presented in Fig. 16, several variants on MDP were computed and are presented in Table 7 with estimated 95% confidence intervals. First, the already discussed narrow bin MDP is given. The second and third columns of Table 7 contain integrated measures of MDP, the overall sound pressure level (OASPL), and A-weighted overall sound pressure level (AOASPL). In both cases, the integration of the noise floor was completed over the individual 1/3 octave bands from 20 Hz–20 kHz, with A-weighting [31] also employed in the latter case prior to final summation. Every microphone had an MDP more than 3 dB below the specification of 93 dB OASPL. The A-weighted MDP is lower in all cases because A-weighting de-emphasizes noise contributions at frequencies below 1 kHz, where the MDP spectra are the highest.

Table 8 Realized MEMS piezoelectric microphone performance compared to specifications and benchmark Kulite sensor

Metric	Obtained	Target Specification	Kulite LQ-1-750-25SG
Sensing element size	ϕ690–828 μm	$\phi \leq 1.9$ mm	864×864 μm^2
Sensitivity	32–44 μV/Pa	500 μV/Pa[a]	1.1 μV/Pa
MDP	40–51 dB[b]	$\leq$ 48.5 dB[b]	48.5 dB[b]
	83–89 dB OASPL	$\leq$ 93 dB OASPL	93 dB OASPL
PMAX[c]	>171.6 dB SPL[d]	$\geq$ 172 dB SPL	$\approx$168 dB SPL
Bandwidth[e]	69 Hz[d]–20 kHz+	20 Hz–20 kHz	<20 Hz–20 kHz+

[a]With on-board gain.
[b]1 Hz bin centered at 1 kHz.
[c]3% distortion.
[d]Microphone J3-F.
[e]±2 dB.

VI. Conclusions

This study focused on the development of microelectromechanical systems (MEMS) piezoelectric microphones with the performance characteristics needed to enable superior technical measurements in full-scale flight tests. Overviews of microphone operation and design were given, together with a detailed account of fabrication, packaging, and experimental characterization.

Characterization results generally met or exceeded target specifications. The collected microphone performance characteristics, as compared both to target specifications and the Kulite microphone presently in-use for full-scale flight tests at the Boeing Company, are presented in this paper (Table 8). Most notably, the MEMS piezoelectric microphones were well under the 48.5 dB sound pressure level (SPL)/93 dB overall sound pressure level (OASPL) minimum detectable pressure (MDP) specification (save for the outlier I8-E) and had a lower noise floor with higher sensitivity (up to 40 times greater) than the Kulite microphones. All of the microphones had a 3% distortion limit above 160 dB SPL. Of the two microphones tested at even higher SPLs, one (J3-F) demonstrated PMAX $\geq$ 171.6 dB SPL. It was not possible to confirm a distortion limit $\geq$ 172 dB due to distortion in the MEMS and reference microphones, but the measurement was highly suggestive that J3-F met the specification. An onboard gain of slightly over 20 dB is sufficient to reach the sensitivity target of 500 μV/Pa. Although the measured $f_{-2\,\mathrm{dB}}$ point of 70 Hz slightly exceeded the 20 Hz minimum target, $f_{+2\,\mathrm{dB}} \geq 20$ kHz was met. Measured microphone resonant frequencies exceeding 100 kHz suggested a surplus of usable bandwidth that could expand the range of applications for the MEMS piezoelectric microphone to model-scale tests. Finally, even the diaphragm of the largest microphone tested, having a diameter of 828 μm (design F), was smaller than the Kulite diaphragm (864 μm on a side) and was less than half of the maximum diameter target specification (1.9 mm).

Future work remains in order to transition the MEMS piezoelectric microphone described here into active duty in aircraft fuselage arrays. Robustness to moisture and freezing, in addition to temperature stability in the range of −60°F to 150°F must be determined. Environmental measurements already underway at the Boeing Company will lead to design improvements or compensation schemes as necessary. In addition, the development of a surface-mount-packaging scheme that is low cost, robust, and extremely thin, with enhanced shielding of electromagnetic interference, is needed.

Acknowledgments

The authors would like to thank the Boeing Company for funding this study and Avago Technologies for the microphone fabrication. Matthew D. Williams and Benjamin A. Griffin would like to acknowledge support from the National Science Foundation for a portion of this study in the form of a pair of Graduate Research Fellowships. Benjamin A. Griffin and Mark Sheplak acknowledge additional support from the Florida Center for Advanced Aero-Propulsion. Sandia National Laboratories is a multiprogram laboratory managed and operated by Sandia Corporation, a wholly owned subsidiary of Lockheed Martin Corporation, for the U.S. Department of Energy's National Nuclear Security Administration under contract DE-AC04-94AL85000.

References

[1] U.S. Government, "Aeronautics and Space, Noise Standards: Aircraft Type and Airworthiness Certification," Title 14 US Code of Federal Regulations, pt. 36, 2004.

[2] Burnett, B., "Ssshh, We're Flying a Plane Around Here," *Boeing Frontiers*, Vol. 4, No. 8, Jan. 2006.

[3] Mengle, V. G., Ganz, U., Bultemeier, E. J., and Calkins, F. T., "Clocking Effects of Chevrons with Azimuthally-Varying Immersions on Shockcell/Cabin Noise," *Proceedings of the 29th AIAA Aeroacoustics Conference*, AIAA Paper 2008-3000, 2008, pp. 1–14.

[4] International Transport WorkersÕ Federation, "Occupational Safety and Health Protections for Cabin Crew Members," Montreal, Canada, International Civil Aviation Organization Working Paper A36-WP/208, Sept. 2007.

[5] Viswanathan, K., "Investigation of Noise Source Mechanisms in Subsonic Jets," *AIAA Journal*, Vol. 46, No. 8, Aug. 2008, pp. 2020–2032. doi:10.2514/1.34471

[6] Herkes, W. H., Olsen, R. F., and Uellenberg, S., "The Quiet Technology Demonstrator Program: Flight Validation of Airplane Noise-Reduction Concepts," *Proceedings of the 12th AIAA/CEAS Aeroacoustics Conference (27th Aeroacoustics Conference)*, Cambridge, MA, AIAA Paper 2006-2720, May 8–10, 2006, pp. 1–9.

[7] Herkes, W., Nesbitt, E., Callender, B., Janardan, B., Moe, J., and Yu, J., "The Quiet Technology Demonstrator Program : Static Test of Airplane Noise-Reduction Concepts," *Proceedings of the 13th AIAA/CEAS Aeroacoustics Conference (28th AIAA Aeroacoustics Conference)*, Rome, Italy, AIAA Paper 2007-3670, May 21–23, 2007, pp. 1–11.

[8] Kulite Semiconductor Products, Inc., "Thin Line IS® Pressure Transducer," http://www.kulitesensors.com.cn/pdf_Data_Sheets/LQ-080.125.pdf [retrieved May 2011].

[9] Bultemeier, E. J., Ganz, U., Premo, J., and Nesbitt, E., "Effect of Uniform Chevrons on Cruise Shockcell Noise," *Proceedings of the 12th AIAA/CEAS Aeroacoustics Conference (27th AIAA Aeroacoustics Conference)*, Cambridge, MA, AIAA Paper 2006-2440, May 8–10, 2006, pp. 1–15.

[10] Arnold, D. P., Nishida, T., Cattafesta, L. N., and Sheplak, M., "A Directional Acoustic Array Using Silicon Micromachined Piezoresistive Microphones," *Journal of the Acoustical Society of America*, Vol. 113, No. 1, Jan. 2003, pp. 289–298. doi:10.1121/1.1527960

[11] Sheplak, M., Seiner, M., Breuer, K. S., and Schmidt, M. A., "A MEMS Microphone for Aeroacoustic Measurements," *Proceedings of 37th AIAA Aerospace Sciences Meeting*, AIAA Paper 1999-0606, Jan. 1999.

[12] Arnold, D. P., Gururaj, S., Bhardwaj, S., Nishida, T., and Sheplak, M., "A Piezoresistive Microphone for Aeroacoustic Measurements," *Proceedings of ASME IMECE 2001 International Mechanical Engineering Congress and Exposition*, New York, NY, ASME Paper MEMS-23841, Nov. 11–16, 2001, pp. 281–288.

[13] King, P. J., and Underbrink, J. R., "Characterization of a Micro-electromechanical Systems (MEMS) Microphone," *Proceedings of the 14th AIAA/CEAS Aeroacoustics Conference*, AIAA Paper 2008-2912, May 2008.

[14] Horowitz, S., Nishida, T., Cattafesta, L., and Sheplak, M., "Development of a Micromachined Piezoelectric Microphone for Aeroacoustics Applications," *Journal of the Acoustical Society of America*, Vol. 122, No. 6, Dec. 2007, pp. 3428–3436. doi:10.1121/1.2785040

[15] Martin, D. T., Jian, L., Kadirvel, K., Fox, R. M., Sheplak, M., and Nishida, T., "A Micromachined Dual-Backplate Capacitive Microphone for Aeroacoustic Measurements," *Journal of Microelectromechanical Systems*, Vol. 16, No. 6, Dec. 2007, pp. 1289–1302. doi:10.1109/JMEMS.2007.909234

[16] Scheeper, P. R., Nordstrand, B., Gullov, B. L. J. O., Clausen, T., Midjord, L., and Storgaard-Larsen, T., "A New Measurement Microphone Based on MEMS Technology," *Journal of Microelectromechanical Systems*, Vol. 12, No. 6, 2003, pp. 880–891. doi:10.1109/JMEMS.2003.820260

[17] Huang, C., Naguib, A., Soupos, E., and Najafi, K., "A Silicon Micromachined Microphone for Fluid Mechanics Research," *Journal of Micromechanics and Microengineering*, Vol. 12, No. 6, 2002, pp. 767–774. doi:10.1088/0960-1317/12/6/307

[18] Kadirvel, K., Taylor, R., Horowitz, S., Sheplak, M., and Nishida, T., "Design and Characterization of MEMS Optical Microphone for Aeroacoustic Measurement," *Proceedings of 42nd Aerospace Sciences Meeting and Exhibit*, AIAA Paper 2004-1030, Jan. 2004.

[19] Mengle, V. G., Ganz, U., Nesbitt, E., Bultemeier, E. J., and Thomas, R., "Flight Test Results for Uniquely Tailored Propulsion-Airframe Aeroacoustic Chevrons: Shockcell Noise," *Proceedings of the 27th AIAA Aeroacoustics Conference*, AIAA Paper 2008-3000, May 2008.

[20] Trolier-McKinstry, S., and Muralt, P., "Thin Film Piezoelectrics for MEMS," *Journal of Electroceramics*, Vol. 12, Nos. 1/2, Jan. 2004, pp. 7–17. doi:10.1023/B:JECR.0000033998.72845.51

[21] Prasad, S. A. N., Gallas, Q., Horowitz, S., Homeijer, B., Sankar, B. V., Cattafesta, L. N., and Sheplak, M., "Analytical Electroacoustic Model of a Piezoelectric Composite Circular Plate," *AIAA Journal*, Vol. 44, No. 10, Oct. 2006, pp. 2311–2318. doi:10.2514/1.19855

[22] Williams, M. D., Griffin, B. A., Reagan, T. N., Underbrink, J. R., and

Sheplak, M., "A MEMS Piezoelectric Microphone for Aeroacoustic Applications," *Journal of Microelectromechanical Systems*, Vol. 21, No. 2, 2012, pp. 270–283. doi:10.1109/JMEMS.2011.2176921

[23] Ruby, R., Bradley, P., Oshmyansky, Y., Chien, A., and Larson, J., "Thin Film Bulk Wave Acoustic Resonators (FBAR) for Wireless Applications," *Proceedings of the 2001 IEEE Ultrasonics Symposium*, Vol. 1, Oct. 2001, pp. 813–821. doi:10.1109/ULTSYM.2001.991846

[24] Lamers, T. L., and Fazzio, R. S., "Accelerating Development of a MEMS Piezoelectric Microphone," *Proceedings of the ASME 2007 International Design Engineering Technical Conferences & Computers Information in Engineering Conference*, ASME Paper DETC2007-34958, Sept. 2007, pp. 593–601.

[25] Fazzio, R. S., Lamers, T., Buccafusca, O., Goel, A., and Dauksher, W., "Design and Performance of Aluminum Nitride Piezoelectric Microphones," *14th International Conference on Micro-Sensors, Actuators and Microsystems*, IEEE, Lyon, France, Jun. 10–14, 2007, pp. 1255–1258.

[26] Mueller, T. J. (ed.), *Aeroacoustic Measurements*, Springer-Verlag, Berlin, 2002, pp. 98–217, Chap. 3.

[27] Alexander, D., Barnard, C., Sheplak, M., and Griffin, B., "Characterization of a High-Frequency Pressure-Field Calibration Method," *Proceedings of the 159th Meeting of the Acoustical Society of America*, Acoustical Society of America, Baltimore, MD, April 19–23, 2010.

[28] Wong, G. S. K., and Embleton, T. F. W., *AIP Handbook of Condensor Microphones*, American Institute of Physics, New York, 1995, pp. 145–161, Chap. 8.

[29] Boulet, B., *Fundamentals of Signals and Systems*, Vol. 1, Da Vinci Engineering Press, Massachuesetts, 2006, Chap. 4.

[30] Dieme, R., Bosman, G., Sheplak, M., and Nishida, T., "Source of Excess Noise in Silicon Piezoresistive Microphones," *Journal of the Acoustical Society of America*, Vol. 119, No. 5, May 2006, pp. 2710–2720. doi:10.1121/1.2188367

[31] Harris, C. M., *Handbook of Acoustical Measurements and Noise Control*, 3rd ed., Acoustical Society of America, New York, 1998, pp. 1.1–1.29, Chap. 1.

M. Glauser
Associate Editor